

Lithium isotopes in population II dwarfs

L. Piau¹

University of Chicago, LASR, 933, East 56th street, Chicago, Il, 60637, USA

ABSTRACT

We investigate the history of ${}^6\text{Li}$ and ${}^7\text{Li}$ in population II dwarfs during the pre main sequence and main sequence. The evolution is followed using the CESAM code and taking into account the most recent physics. The effective temperature ranges from ≈ 4700 K to ≈ 6400 K and therefore concerns objects on the so-called Spite plateau and cooler. We find the ${}^7\text{Li}$ pre main sequence depletion is unable to account for the observations in the halo whatever the effective temperature. This supports microscopic diffusion and an additional non standard mixing process both acting during the main sequence. On the contrary the models ${}^6\text{Li}$ pre main sequence depletion appears too strong and is marginally compatible with recent detections.

During the main sequence we introduce the effects of tachocline diffusion. This process is a rotationally induced mixing acting at the top of the radiative core. We show that the differences in the early rotation history cannot result in scattered lithium abundances on the Spite plateau. Moreover the tachocline mixing process predicts ${}^7\text{Li}$ abundances in good agreement with the observations. We briefly address the question of turn off ${}^7\text{Li}$ poor stars. A modest accretion of lithium free matter would be enough to explain their low abundance in this element.

We expect the scatter in ${}^7\text{Li}$ abundances is correlated to variations in $[\text{Fe}/\text{O}]$ ratio for dwarfs cooler than 5500 K. Finally the tachocline mixing is robust with respect to the recent ${}^6\text{Li}$ observations around the turn-off. We similarly suggest the $[\text{Fe}/\text{O}]$ should be higher in objects with ${}^6\text{Li}$ and effective temperature below 6000 K.

Subject headings: stars: population II — stars: light elements — stars : internal mixing

1. Introduction

Lithium, beryllium, and boron isotopes get destroyed by proton capture in stellar interiors between $2 \cdot 10^6$ K and $5 \cdot 10^6$ K. Therefore their surface abundances allow direct measurement of the depth of the outer convection zones. In addition when the temperature near the base of a convection zone (hereafter BCZ) is too low they permit to set constraints on any process that would mix the matter beneath. The light elements have been extensively observed in main sequence low mass stars. With asteroseismology they are currently the only means to constrain low mass dwarfs' interiors.

Population II main sequence stars being the oldest non-evolved objects, they should reflect the initial chemical conditions of our Galaxy. It is therefore particularly interesting to set constraints

on their possible surface abundance changes since they were formed. In particular ${}^7\text{Li}$ has been extensively studied in these objects both from theoretical and observational viewpoints. ${}^7\text{Li}$ is one of the rare nucleids that was synthesised through Big Bang Nucleosynthesis (hereafter BBN) in an observable amount. Estimating its initial abundance from observations of the oldest stars provides essential indications on the conditions in the primordial Universe. More than 20 years ago Spite & Spite (1982) found that most halo field stars with $[\text{Fe}/\text{H}] < -1.5\text{dex}$ and $5500\text{K} < T_{\text{eff}} < 6300\text{K}$ display similar ${}^7\text{Li}$ abundances. Since then this result was confirmed by many other observations (Hobbs & Duncan 1987; Spite & Spite 1993; Thorburn 1994; Ryan et al. 1996). The ${}^7\text{Li}$ abundance on the so-called Spite plateau is now estimated to lie around 2.0-2.2 dex with a very small intrinsic scatter below 0.1 dex. The key issue for stellar physi-

cists is the determination of how this abundance has changed since the halo stars were formed.

Recently, new spectrographs such as UVES on the VLT have considerably increased the number of measurements in other light elements isotopes such as ^6Li (Asplund et al 2005a, 2005b) and ^9Be . This makes the determination of their evolution from the modelling point of view relevant. In contrast to ^7Li , these nucleids are not produced in a significant manner through BBN but are the result of fusion or spallation processes in the interstellar medium as suggested by the pioneering work of Reeves et al. (1970). Beside this they have different depletion temperatures than ^7Li so that they provide complementary information on stellar structure and evolution. ^6Li is especially intriguing as present measurements suggest it does not evolve over a broad range of metallicity (Asplund et al. 2005a) whereas it is expected to increase substantially due to production by low energy cosmic rays (Vangioni-Flam et al. 1999).

In this work we present the predictions of models of population II low mass stars on the ^6Li and ^7Li surface abundances. The models are evolved up to 13 Gyr, a plausible age for halo stars having $[\text{Fe}/\text{H}]=-2$ dex (VandenBerg 2000). The history of the isotopes is investigated both on the pre main sequence (hereafter pre MS) and the main sequence (hereafter MS) using the most recent physics in terms of nuclear reaction rates, equation of state and opacities. We have, moreover, studied the effects of the rotationally induced tachocline mixing. This process has given encouraging results for the evolution of light elements on the surface of population I solar analogs but has never been studied in population II objects. The paper is organized as follows : in §2 we describe in detail the general inputs to our code and the assumed initial composition. The rotation history has been followed in detail. In §3 we present our assumptions on the rotation history and consequently on the tachocline mixing process. Sections 4 and 5 respectively investigate the effects of pre MS and MS history on ^6Li and ^7Li . Finally we discuss our results in §6.

2. The evolutionary code and general inputs

We use the CESAM code to perform the computations (Morel 1997). This hydrostatic onedimensional code has been extensively employed to model various stellar types and stages of evolution over the last decade. It has also been used in solar structure computations and helio/asteroseismology¹. Various adaptations have been made to the code in order to use the most adequate inputs for the present issue.

The equation of state: in the case of population II objects the metals' impact on the equation of state (EOS) is negligible. Consequently we use the OPAL2001 EOS tables for pure hydrogen-helium mixtures² (Rogers & Nayfonov 2002).

The opacities: consistent with the EOS, we use the OPAL opacities. The opacity table considered is the α -element enhanced table of F. Allard. For this table $[\alpha/\text{Fe}] = 0.3\text{dex}$ where α stands for the α -elements (see hereafter). Low temperature opacity tables are based on computations similar to Alexander and Ferguson (1994). Below $\log T = 3.75$ the OPAL opacity tables are replaced by the tables provided by J. Ferguson (private communication). These tables were generated for the same intermetallic ratios as those of the OPAL opacity tables.

The nuclear reactions: we use the NACRE compilation of nuclear reaction rates (Angulo et al. 1999). Our network includes the proton-proton chains and CNO cycle. Furthermore the $^6\text{Li}(p, \alpha)^3\text{He}$ and $^9\text{Be}(p, ^2\text{H})^2^4\text{He}$ reactions are taken into account.

The atmosphere modelling: the outer boundary conditions to the stellar structure equations are provided using the Nextgen atmosphere models. The atmospheric temperature-optical depth relations have kindly been computed by P. Hauschildt for the required composition and on a grid that spans the effective temperature-surface gravity domain we encounter.

The convection: the convection zones are assumed to be fully homogeneous, and modeled using the mixing-length theory (hereafter MLT) in

¹The list of the scientific publications using CESAM is available at <http://www.obs-nice.fr/cesam/>

²Available at <http://www-phys.llnl.gov/Research/OPAL/>

a formalism almost identical to that of Böhm-Vitense (1958). This formalism is precisely described in the appendix of Piau et al. (2005). We have considered $\alpha_{\text{MLT}} = 1.766$ which is our Sun-calibrated value.

The diffusion processes: The microscopic diffusion is taken into account following the Michaud & Proffitt (1993) prescriptions. The details of the tachocline diffusion process are given in §3.

In addition to these different points the initial composition is an essential question. For instance, the impact of metallicity on the extension of convection during the pre MS is a priori unknown. This impact is strong in the case of population I object (Piau & Turck-Chièze 2002, hereafter PTC02). Moreover in MS models changing the intermetallic ratios affects the temperature at the base of the convection zone for a given effective temperature. Both phenomena could significantly change the light elements' histories. We assume $[\text{Fe}/\text{H}] = -2.0$ dex and $[\alpha/\text{Fe}] = +0.3$ dex. α stands for the oxygen and the usual α -elements (Ne, Mg, Si, S, Ar, Ca and Ti). We consider a similar ratio for nickel and chromium as for iron while manganese and aluminum are supposed underabundant by 0.15 dex and 0.30 dex with respect to iron (Gratton 1989; Magain 1989). Recent observations of the $[\text{C}/\text{O}]$ vs $[\text{O}/\text{H}]$ function in halo stars (Akerman et al. 2004) suggest that the carbon is underabundant with respect to oxygen there. The deficiency being around 0.4 dex for the oxygen fraction accounted in our models it would bring the carbon to iron ratio close to solar. We have thus considered $[\text{C}/\text{Fe}] = 0$ which is also in agreement with other studies regarding carbon in population II (McWilliam 1995). ³ Nitrogen is assumed to follow the same trend as carbon so that $[\text{N}/\text{Fe}] = 0$. The total helium mass fraction along with the ratios of ²H, ³He, and ⁷Li to ¹H are set to their primordial values following the recent BBN calculations of Coc et al. (2004). We consider that ⁶Li = 1.13 dex and ⁹Be = -0.15 dex initially which is adapted from the observations of turn-off population II stars by Cayrel et al. (1999) and Pasquini et al. (2004) respectively. In both last cases we

increase the observed abundances by 0.2 dex in order to compensate for the microscopic diffusion at the halo age. ⁹Be surface abundance is followed, however because of the higher temperature for ⁹Be proton capture it is never affected by nuclear reactions on our range of T_{eff} . We therefore shall not discuss ⁹Be any further in this study. The tables 1 and 2 provide the detailed composition. Hydrogen and helium mass fractions are $X = 0.7518$ and $Y = 0.2479$ respectively. Unless explicitly mentioned we always adopt this composition.

3. The rotation

Population II stars cannot be observed during their evolution. Thus it is impossible to observe their surface rotation history. Currently all the main sequence population II stars exhibit very low equatorial velocities. The line broadening due to these rotation rates is comparable to the spectrographs resolution today and for most objects only upper limits of the projected equatorial velocities are accessible. Studying 9 halo stars Smith et al. (1998) found $v_{\text{ini}} < 3 \text{ km.s}^{-1}$ for all of them. Even this upper limit was lowered to 2 km/s by more recent observations (see Fig. 1 of Ryan et al. 2002). Interestingly, the latter authors also report that 3 stars out of their sample exhibit slightly higher v_{ini} in the 5.5 to 8.3 km.s^{-1} range. These peculiar stars are spectroscopic binaries. They exhibit ⁷Li surface abundances at least 0.5 dex below the other objects and should not be considered when studying the isolated stars general lithium history we address here. However we briefly touch on the question of such Li-poor objects in §5.

We compute the rotation evolution by applying different assumptions to the angular momentum losses and internal transport for a $0.7M_{\odot}$ model. With $T_{\text{eff}} = 5890\text{K}$ at 13 Gyr this star lies in the middle of the Li-plateau. Four different models of rotation were built. In the following subsections we present our assumptions on the rotation history. First we discuss our choices of surface angular momentum loss laws that in turn determine the surface rotation. Second we address the question of the inner radiation core rotation that is the relevant quantity for the tachocline diffusion efficiency. Third we briefly describe the way tachocline mixing was implemented.

³The situation seems different in extremely metal poor stars ($-4.1 < [\text{Fe}/\text{H}] < -2.7$ dex) where $[\text{C}/\text{Fe}]$ or $[(\text{C}+\text{N})/\text{Fe}]$ is close to 0.2 dex (Cayrel et al. 2004, Spite et al. 2005). However, only the objects with $[\text{Fe}/\text{H}]$ around -2.0 dex are within the scope of this work.

Table 1: Metal fractions relative to the Sun.

Metals	[X/H]
O,Ne,Na,Mg,Si,P,S,Cl,Ar,Ca,Ti	-1.7
Fe,Ni,Cr,C,N,K	-2.0
Mn	-2.15
Al	-2.30

Table 2: Light element number abundances relative to hydrogen adapted from Coc et. al (2004) except for ${}^6\text{Li}$ and ${}^9\text{Be}$ (see text). Following Coc et. al (2004) we consider the helium mass fraction to be $Y=0.2479$.

ratios	${}^2\text{H}/{}^1\text{H}$	${}^3\text{He}/{}^1\text{H}$	${}^6\text{Li}/{}^1\text{H}$	${}^7\text{Li}/{}^1\text{H}$	${}^9\text{Be}/{}^1\text{H}$
values	$2.60 \cdot 10^{-5}$	$1.04 \cdot 10^{-5}$	$1.34 \cdot 10^{-11}$	$4.15 \cdot 10^{-10}$	$7.07 \cdot 10^{-13}$
values (log)	-4.58	-4.98	1.13	2.62	-0.15

3.1. The surface rotation

We make the assumption that population II low mass stars experience an evolution of surface rotation which is similar to their population I counterparts:

i) The star initially rotates as a solid body and following Bouvier et al. (1997) (hereafter BFA97) we consider an initial rotational period of $P_o = 8$ days. This period remains unchanged until the star decouples from its initial accretion disk which we assume occurs at $\tau_d = 3$ Myr (case A) or 0.5 Myr (case B).

ii) Once the star is no longer locked to its disk the angular momentum decreases following the Kawaler (1988) prescription.

$$\frac{dJ}{dt} = -K\Omega^3 \left(\frac{R}{R_\odot}\right)^{1/2} \left(\frac{M}{M_\odot}\right)^{-1/2} \text{ if } \Omega < \Omega_{\text{sat}} \quad (1)$$

$$\frac{dJ}{dt} = -K\Omega\Omega_{\text{sat}}^2 \left(\frac{R}{R_\odot}\right)^{1/2} \left(\frac{M}{M_\odot}\right)^{-1/2} \text{ if } \Omega > \Omega_{\text{sat}} \quad (2)$$

K is set to $K_\odot = 3.25 \cdot 10^{47} \text{g.s.cm}^2$ (cases A and B) which leads to the actual solar rotation for a solar model. For case C we take $K = K_\odot/10$. This second value yields a 1.6km.s^{-1} equatorial velocity at 13 Gyr which is nearly the maximum velocity allowed by current observations ($v \sin i <$

2km.s^{-1}). The surface magnetic activity saturates around $10\Omega_\odot$. The actual threshold $\Omega_{\text{sat}} = 14\Omega_\odot$ ($3.78 \cdot 10^{-5} \text{rad.s}^{-1}$) is accurately tuned from the rotation observations in middle aged open-clusters (BFA97).

iii) To compute the rotational rate inside the radiation zone we explore two possibilities regarding its coupling to the convective envelope. Firstly we consider that these regions are instantaneously coupled so that the whole star rotates as a solid always (cases A, B, C). Secondly we consider the radiative and convective zones to rotate as solids but not necessarily with the same speeds (case D, see the next subsection).

The four empirical parameters ($P_o, \tau_d, \Omega_{\text{sat}}, K$) in the rotation law we adopt are directly calibrated from the observations on our Sun and population I solar analogs. It seems reasonable to assume similar angular momentum losses through magnetic braking for solar analogs and Li-plateau stars. The reason is that, in terms of surface conditions or convection zone extension, the Sun is quite comparable to our $0.7M_\odot$ population II $[\text{Fe}/\text{H}] = -2$ dex model. At 13 Gyr we find for this object : $T_{\text{eff}} = 5890 \text{K}$, surface gravity = $1.36 g_\odot$ and $0.764 R_\star$ as radius for the radiative core vs $0.713 R_\odot$ for the actual Sun (global properties of plateau stars as a function of their masses can be found in Proffitt & Michaud 1991). We consequently apply the braking law parameters from BFA97. The

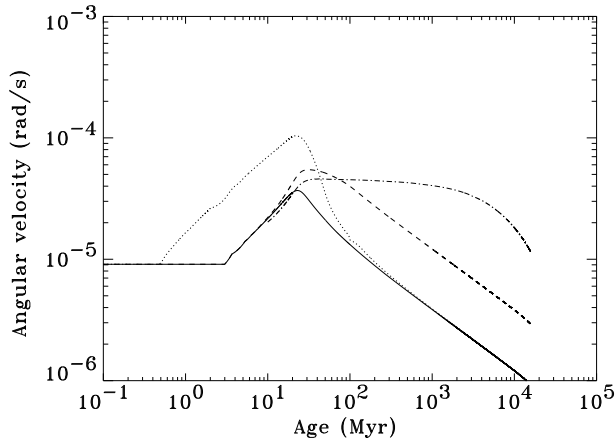


Fig. 1.— Radiation zone angular velocity vs age for a $0.7M_{\odot}$ model. The solid body rotation models are shown by the solid line : $K = K_{\odot}$, and $\tau_d = 3$ Myr (case A); the dotted line : $K = K_{\odot}$, and $\tau_d = 0.5$ Myr (case B); the dashed line : $K = K_{\odot}/10$, and $\tau_d = 3$ Myr (case C). Dot-dashed line represents the differential rotation model with $K = K_{\odot}$, $\tau_d = 3$ Myr and $\tau_c = 1$ Gyr (case D). The difference between the case A and case B models is related to early conditions and vanishes after ~ 500 Myr.

shorter P_o and/or τ_d the higher zero age main sequence (hereafter ZAMS) rotation velocity (figure 1). Then a higher Ω_{sat} implies a slower pace for rotational slow-down during early MS. To study the effects of fast ZAMS rotation we built a model with $\tau_d = 0.5$ Myr. We stress however that none of the three parameters (P_o , τ_d and Ω_{sat}) has a significant impact on rotation after ~ 0.5 Gyr where, in contrast, the K parameter plays a major role. K determines the star’s asymptotic velocity. Considering $\tau_d = 3$ Myr, we explore its impact when it is varied from K_{\odot} to $K_{\odot}/10$ for which it causes surface rotation velocities to vary from ~ 0.6 to $\sim 1.7\text{km.s}^{-1}$ at 13 Gyr (figure 1).

3.2. The internal rotation

The rotational rate in the upper radiation zone is the relevant quantity for the tachocline diffusion computation. This rate is also the surface rotation rate when the rotation is solid. In the case of population I solar like stars there is an accumulation of observational and theoretical clues suggesting that this should be correct during most

of the main sequence. Helioseismic observations show that our Sun rotates nearly as a solid at least down to $0.2R_{\odot}$ (Thompson et al. 2003). As shown in Piau et al. (2003), the surface rotation history in the young clusters does not seem compatible with differential rotation with the radius. In this last work we came to the conclusion that solid body rotation was certainly achieved as early as the Hyades age. Furthermore one would expect more significant surface magnetic activity in young slow rotators if they had fast spinning cores (BFA97). Finally some recent models of angular momentum transport by internal waves suggest an efficient rigidification of the stellar interior both for the Sun (Talon, Kumar & Zahn 2002) and for the lithium plateau stars (Talon & Charbonnel 2004).

In the case of lithium plateau stars however we cannot completely exclude differential rotation with depth because part of the low metallicity horizontal branch (hereafter HB) stars show significant surface rotation while on the other hand the turn off halo stars are extremely slow rotators. We therefore built a rotation model assuming $K = K_{\odot}$, $\tau_d = 3$ Myr and $\tau_c = 1$ Gyr. For this model, during the time interval dt , the radiative core and the convective envelope exchange an angular momentum fraction $dJ = \frac{\Delta J}{\tau_c} dt$.

$$\Delta J = \frac{(I_{\text{env}}J_{\text{core}} - I_{\text{core}}J_{\text{env}})}{I_{\text{core}} + I_{\text{env}}}$$

is the angular momentum exchange that would achieve synchronisation of the core and the envelope, τ_c is therefore a coupling timescale for rotation between these regions. As shown on figure 1 this option yields to a significant increase of the rotation rate in the radiation zone. At 13 Gyr the core of the $0.7M_{\odot}$ star rotates at $1.35 \cdot 10^{-5} \text{rad.s}^{-1}$ while the surface rotation velocity linear is 1.5km.s^{-1} .

For this model the radiative core rotates ~ 5 times faster than the envelope. Indeed this high ratio could be expected from constraints on fast rotating HB stars. The coolest HB stars ($T_{\text{eff}} < 12000\text{K}$) are spinning as fast as 40km.s^{-1} (Behr 2003). Sills and Pinsonneault (2000) made a systematic study of the angular momentum history during the red giant branch evolution. Their models save the greatest amount of angular momentum when specific angular momentum is constant

in the convective envelope and fully retained in the radiative core. For this situation the authors demonstrated that the fast rotating HB stars could be accounted for if turn-off progenitors rotate at 4km.s^{-1} . The subsequent observations of Ryan et al. (2002) suggest $v_{\text{ini}} < 2\text{km.s}^{-1}$ however. Thus if these turn-off stars rotate as solid bodies their low angular momentum seems difficult to reconcile with the high rotation velocities of the HB stars even for very favorable conditions of angular momentum distribution. We can estimate the rotational velocity of the core for a $0.8M_{\odot}$ turnoff star under the following hypotheses: i) The total angular momentum of the star is similar to its HB value : $J_{\text{HB}} = J_{\text{core}} + J_{\text{env}}$. J_{HB} , J_{core} and J_{env} respectively stand for the angular momenta of all the HB star, its turn off progenitor core and envelope. ii) Both the whole HB star and the radiative core of its turn off progenitor rotate as solids. iii) The surface velocities of the HB star and its turn off progenitor are respectively 40km.s^{-1} and 2km.s^{-1} .

Then

$$\Omega_{\text{core}} = \frac{I_{\text{HB}}\Omega_{\text{HB}} - I_{\text{env}}\Omega_{\text{env}}}{I_{\text{core}}} \quad (3)$$

At 11.8 Gyr when central hydrogen exhaustion occurs ($X_{\text{c}} = 10^{-3}$) $I_{\text{core}} = 4.08 \cdot 10^{53} \text{g.cm}^2$, $I_{\text{env}} = 3.71 \cdot 10^{51} \text{g.cm}^2$, and $\Omega_{\text{env}} = 2.45 \cdot 10^{-6} \text{rad.s}^{-1}$. The rotation rate of the core is thus $\Omega_{\text{core}} = 3.38 \cdot 10^{-5} \text{rad.s}^{-1}$. Now if we compute the rotational evolution of this $0.8M_{\odot}$ model with the case D parameters we find $\Omega_{\text{core}} = 4.71 \cdot 10^{-5} \text{rad.s}^{-1}$ at the same age. Both evaluations are quite comparable.

Before moving to the rotation effects in the next sections let us sum up our four different assumptions on rotation and what motivates them :

Case A): Solid body rotation, $K = K_{\odot}$, and $\tau_{\text{d}} = 3 \text{Myr}$. This rotation model is calibrated thanks to the Sun and population I observations. Unless explicitly mentioned we will always use this rotational law.

Case B): Solid body rotation, $K = K_{\odot}$, and $\tau_{\text{d}} = 0.5 \text{Myr}$.

Case C): Solid body rotation, $K = K_{\odot}/10$, and $\tau_{\text{d}} = 3 \text{Myr}$. Cases B) and C) evaluate the impact of increased rotation rates with respect to case A) either because of lower angular momentum losses or higher ZAMS rotation speed.

Case D): Differential rotation model $K = K_{\odot}$, and $\tau_{\text{d}} = 3 \text{Myr}$. The coupling time scale between the convective envelope and the radiative core is $\tau_{\text{c}} = 1 \text{Gyr}$. This model aims at evaluating the effects of a possible fast rotating core.

3.3. The tachocline mixing

The transition region between the solar convective and radiative zones shows sharp variations of the rotation velocity with depth and has therefore received the name of tachocline. There rotation and differential rotation with latitude induce a slow mixing (Spiegel & Zahn 1992). The tachocline mixing has been introduced in modelling studies about the Sun and population I solar-like stars (Brun et al. 1999, 2002; Piau et al. 2003). It produces better agreement between theoretical and observed sound speed and explains the ${}^7\text{Li}$ and ${}^9\text{Be}$ main sequence histories. However, the tachocline mixing effect has never been systematically studied in population II stars.

We presented in detail our assumptions on the global rotation history hereabove. The differential rotation $\tilde{\Omega}$ with latitude in the convection zone is then deduced assuming it is the solar differential rotation for the solar rotation rate and otherwise scales as $\Omega^{0.7}$ (Donahue, Saar & Baliunas 1996). It is noteworthy that the tachocline mixing has features making it robust with respect to the present constraints on stellar rotation: it is not related to differential rotation with depth which presently seems excluded in MS stars by observations as well as by new models of internal angular momentum transport. Besides this and contrary to models where angular momentum is extracted by a diffusive process, it infers no ${}^9\text{Be}$ depletion in solar analogs. Our tachocline mixing prescription has two free parameters that must be empirically calibrated: the width of the tachocline and the buoyancy frequency in the tachocline region. The width is calibrated from solar seismic measurements to 2.5% of the total radius. The value of the buoyancy frequency is estimated to be $10 \mu\text{Hz}$. A change to $2 \mu\text{Hz}$ is briefly investigated however (figure 4). A discussion of the choice of these values can be found in Piau et al. (2003).

We do not take into account the tachocline mixing during the pre main sequence (which is considered to end at 200 Myr) unless explicitly mentioned. The reason is that the time for effective

diffusion induced by the tachocline process is the order of :

$$t_{\text{diff}} = 450 \left(\frac{\tilde{\Omega}}{\Omega} \right)^{-1} \text{Myr}$$

(Zahn 2004). Even in the case of extreme differential rotation ($\tilde{\Omega} = \Omega$) this duration thus already exceeds 200 Myr. A detailed description of the tachocline process equations can be found in Zahn (2004).

4. Lithium isotopes during the pre main sequence

During the pre MS, low mass stars presumably evolve from a fully convective state to a radiative core and convective envelope structure. The temperature at the BCZ reaches a maximum which may induce light element depletion visible at the surface (see PTC02 and references therein). The lower the mass (i.e. the lower the ZAMS T_{eff}), the deeper the convection zone at any stage of the evolution and the stronger the light element depletion. We evaluate the pre MS depletion of ^6Li and ^7Li based on models including no tachocline diffusion. The impact of the pre MS evolution is considered at 200 Myr. At this age the proton-proton chains provide more than 99% of the energy while the microscopic diffusion is negligible for all our models. We consider therefore 200 Myr as the end of pre MS. The computations were made for the helium mass fraction $Y=0.2479$ and the metallicities $[\text{Fe}/\text{H}]=-3$ dex, $[\text{Fe}/\text{H}]=-2$ dex (standard case), $[\text{Fe}/\text{H}]=-1$ dex and $[\text{Fe}/\text{H}]=-0.7$ dex. As shown in table 3 and figure 2 no significant ^7Li depletion is induced during pre MS even for objects of ZAMS effective temperature at the cool end of the Spite plateau ($\sim 0.65M_{\odot}$). Below this limit we estimate a depletion phenomenon rapidly increasing as the effective temperature decreases. These predictions are however unable to fully explain the $T_{\text{eff}} - ^7\text{Li}$ pattern presently observed below 5500 K. Firstly in the $T_{\text{eff}} - ^7\text{Li}$ plan, we compute a 0.18 dex ^7Li decrease per 100 K between 5175 K (0.62 M_{\odot} model) and 4975 K (0.58 M_{\odot} model). This slope is smaller than the estimate of 0.27 dex based on observations between 5000 K and 5500 K suggested by Ryan & Deliyannis (1998). Second the predicted depletion rate around 5000 K is clearly lower than what is observed. Finally even the current intensity computed for pre MS ^7Li depletion could be questioned: in the case of

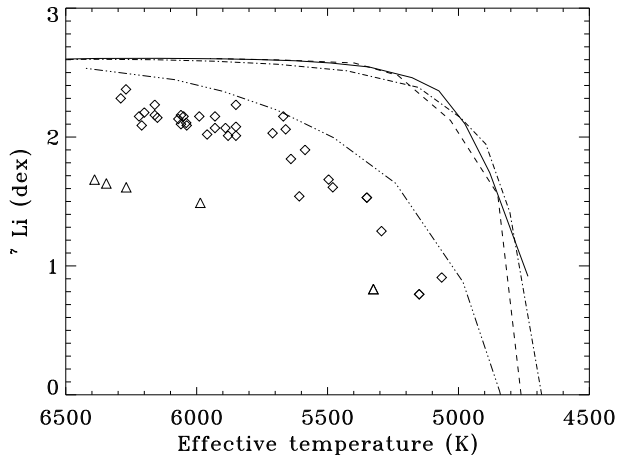


Fig. 2.— ^7Li pre MS depletion at 200 Myr in $[\text{Fe}/\text{H}]=-2$ dex (solid line), $[\text{Fe}/\text{H}]=-1$ dex (dashed line), $[\text{Fe}/\text{H}]=-3$ dex (dash-dotted line) models. These models all exhibit similar pre MS ^7Li depletion patterns. The $[\text{Fe}/\text{H}]=-0.7$ dex models (dash three dotted line) exhibit higher depletion because of the increasing impact of metals on opacity. Observations (diamonds) and upper limits (triangles) are from Ryan et al. (1996), Ryan & Deliyannis (1998), Ryan et al. (1999) and Ryan et al. (2001). For the sake of clarity error bars are not shown.

the population I G-type stars it clearly exceeds what is observed (Ventura et al. 1998; PTC02). We conclude that the $T_{\text{eff}} - ^7\text{Li}$ relation currently observed in the halo stars and for temperatures cooler than the cool end of the Spite plateau was (at least partially) built after the pre MS.

It is interesting to note that the computed pre MS ^7Li depletion does not depend on the metallicity from $[\text{Fe}/\text{H}]=-3$ to $[\text{Fe}/\text{H}]=-1$ dex. As shown on figure 2 the predicted $^7\text{Li} - T_{\text{eff}}$ relations are almost identical on this range of metal fraction. This point is a marked difference from the pre MS population I depletion predictions. Contrary to population I objects the metals represent a very small fraction of the plasma components in the halo dwarfs. Despite the numerous bound-bound and bound-free interactions with the radiation field the contribution of heavy chemical species to the opacity budget near the BCZ becomes small below $[\text{Fe}/\text{H}]=-1$ dex. We computed the metal contribution to the opacity in the $[\text{Fe}/\text{H}]=-0.7$, -1 and -2 dex cases. For this purpose we used the monochro-

Table 3: ZAMS (age = 200 Myr)lithium to initial lithium ratios as function of temperature for microscopic diffusion models : $[\text{Fe}/\text{H}]=-2$ dex and $Y=0.2479$.

Mass (M_{\odot})	0.80	0.75	0.70	0.65	0.62	0.58
ZAMS T_{eff} (K)	6144	5893	5621	5341	5177	4975
${}^7\text{Li}_{\text{ZAMS}}/{}^7\text{Li}_0$	0.97	0.96	0.93	0.83	0.69	0.30
${}^6\text{Li}_{\text{ZAMS}}/{}^6\text{Li}_0$	0.43	0.15	$1.1 \cdot 10^{-2}$	$3.6 \cdot 10^{-6}$	$< 10^{-7}$	$< 10^{-7}$

matic calculations of Iglesias & Rogers (1996). The contribution of a component is computed by subtracting the opacity evaluated for the mixture without the component to the opacity of the global mixture. This requires that the component whose opacity contribution is evaluated does not provide a significantly fraction of the free electrons⁴. Table 4 compares these computations showing the increasing role of metals in the opacity budget with increasing $[\text{Fe}/\text{H}]$.

Being more fragile, ${}^6\text{Li}$ is more strongly affected by the pre MS peak temperatures near the BCZ. We compare here our computations to data collected in Nissen et al. (1999) and mostly Asplund et al. (2005a, 2005b). For this sample we restrict ourselves to the nine stars showing a non-zero ${}^6\text{Li}/{}^7\text{Li}$ isotopic ratio to a 2σ confidence level. In order to account for the microscopic diffusion processes during MS let us recall that our initial ${}^6\text{Li}$ has been increased by 0.2 dex with respect to the 0.93 dex of the Cayrel et al. (1999) measurement in HD84937. Our modelling of pre MS ${}^6\text{Li}$ history suggests features whose consequences are clearly not observed in the present halo stars. First the depletion increases for decreasing effective temperature even in the [6500,6000] K range (figure 3). This trend is not present in the observations, which also systematically suggest a higher abundance than predicted. For instance the metallicity of HD106038 ($T_{\text{eff}} = 5905\text{K}$) is $[\text{Fe}/\text{H}]=-1.35$ dex but this star is almost 2 dex above the $T_{\text{eff}} - {}^6\text{Li}$ track for $[\text{Fe}/\text{H}]=-1$ dex at its effective temperature. Also because the outer convection zones extend closer to the ${}^6\text{Li}$ than the ${}^7\text{Li}$ burning regions the depletion appears to depend on the metallicity between $[\text{Fe}/\text{H}]=-2$ and -1 dex. On the contrary,

observed ${}^6\text{Li}$ abundances appear independent of metallicity : in figure 3 the cases of HD68284 (coolest object) and HD160617 (object closest to 6000 K) are striking. Although they have metallicities of -0.59 dex and -1.76 dex respectively they display similar ${}^6\text{Li}$ fractions. The difference we expect for a 1 dex variation of $[\text{Fe}/\text{H}]$ is over 1.5 dex if $T_{\text{eff}} < 6000\text{K}$. As a matter of fact the data suggest a ${}^6\text{Li}$ plateau with respect to $[\text{Fe}/\text{H}]$ (Asplund 2005a; 2005b). We note that there also seems to be a plateau in the $T_{\text{eff}} - {}^6\text{Li}$ relation. As the depletion rates are too large when compared to this plateau, the situation of ${}^6\text{Li}$ in population II stars is very similar to the situation of ${}^7\text{Li}$ in population I stars regarding pre MS: the actual computations predict an overdepletion (PTC02). Interestingly this discrepancy lingers despite very different compositions and the improvements in the physical inputs to the code.

5. Lithium isotopes during the main sequence

Pre main sequence computations suggest that the ${}^7\text{Li}$ abundance pattern on the Spite plateau or below $T_{\text{eff}} = 5500\text{K}$ was not achieved through early evolution but during the MS. Furthermore ${}^6\text{Li}$ shows no systematic pre MS depletion at least down to $\sim T_{\text{eff}} = 5900\text{K}$. In this section we study the effect of the MS tachocline mixing (Spiegel & Zahn 1992) on both lithium isotopes. Pre MS depletion has been systematically cancelled. Thus we assume that all the stars exhibit on their surface their formation lithium on the ZAMS. This assumption originates from the present computations indicating that ${}^6\text{Li}$ pre MS depletion is overestimated. In order to study correctly the lithium isotopes history during MS one should not include pre MS effects that are not fully understood at the moment.

⁴In this respect we remark that the evaluation of element opacities Table 3 of Piau & Turck-Chièze (2002) is incorrect in the very cases of hydrogen and helium.

Table 4: Opacity and impact of the main metals contributing to the opacity (O, Ne, Mg, Si, S and Fe) at the BCZ. The opacities are computed at the peaks of BCZ temperature (i.e maximum lithium depletion rate) in three objects that end up with similar effective temperatures on the ZAMS. The ZAMS effective temperatures are 4975 K, 4991 K and 4982 K for the $[\text{Fe}/\text{H}]=-2$ dex, -1 dex and -0.7 dex respectively. This temperature corresponds to a moderate ${}^7\text{Li}$ depletion during the pre-MS (see fig 2).

	$[\text{Fe}/\text{H}]=-2$ $M_{\star} = 0.58M_{\odot}$	$[\text{Fe}/\text{H}]=-1$ $M_{\star} = 0.62M_{\odot}$	$[\text{Fe}/\text{H}]=-0.7$ $M_{\star} = 0.70M_{\odot}$
Pre MS maximal BCZ temperature & corresponding density	3.44 10^6K 3.98 g.cm^{-3}	3.45 10^6K 3.95 g.cm^{-3}	3.79 10^6K 2.66 g.cm^{-3}
Opacity (κ)	5.37 $\text{cm}^2.\text{g}^{-1}$	8.95 $\text{cm}^2.\text{g}^{-1}$	7.62 $\text{cm}^2.\text{g}^{-1}$
Contribution of O Ne Mg Si S Fe to κ	7.9 %	43 %	61 %
Contribution of C N Na Al P Cl Ar K Ca Ti Cr Mn Ni to κ	0.4 %	2.6 %	3.9 %

5.1. The ${}^7\text{Li}$ plateau

When coupled to BBN computations, two independent observational facts allow constraints on the primordial ${}^7\text{Li}/{}^1\text{H}$ ratio : the deuterium abundance measurements in quasar absorption systems (Burles 2002 and references therein) and the cosmic microwave background anisotropies probed by the *Wilkinson Microwave Anisotropy Probe* (Cyburt et al. 2003; Coc et al. 2004). These constraints both point towards a similar ${}^7\text{Li}$ fraction ~ 3 times higher than what is observed in halo dwarfs of effective temperature larger than 5500 K (see figure 2). The reason for this discrepancy does not currently seem to originate in uncertainties on the BBN cross sections (Cyburt et al. 2004). The lithium depletion during halo dwarfs evolution therefore remains a plausible explanation. Besides this, if one considers population I stars' histories, a change in the surface abundances is expected for halo dwarfs. Helioseismic measurements strongly support microscopic diffusion in the Sun (Bahcall, Pinsonneault & Wasserburg 1995) i.e. on a shorter timescale and for a deeper convection zone than experienced in Li-plateau objects. Moreover, a non standard mechanism is necessary to explain the time dependent ${}^7\text{Li}$ depletion observed in open-clusters G type stars as well as the actual solar photospheric lithium abundance.

There is no physical reason why such a process should not be at work in population II stars. The interplay of this process with microscopic diffusion sets the global lithium history.

Several mechanisms have been proposed to explain the ${}^7\text{Li}$ depletion in Galactic disk stars and were also applied to halo stars : mass loss (Vauclair & Charbonnel 1995), mixing by internal waves (Montalbán & Schatzman 2000) and rotation effects. These latter mechanisms have been particularly explored notably as during population I MS lifetime both depletion and rotation rates are observed to decrease. Recently Théado & Vauclair (2001) considered the effects of meridional circulation coupled to molecular weight gradient effects. Their models were able to produce a nearly constant ${}^7\text{Li}$ depletion for the stars on the plateau without ad hoc adjustment of their parameters. Pinsonneault et al. (2002) used a rotationally induced mixing model calibrated on the Sun. They found that the scatter observed on the plateau and the small fraction of stars below the plateau were compatible with a mild depletion from 0.1 to 0.2 dex.

Whatever the process responsible for the Spite plateau lithium evolution, this process has to comply with two challenges. First the plateau is remarkably flat with T_{eff} : stars with quite different outer convection zones experience similar deple-

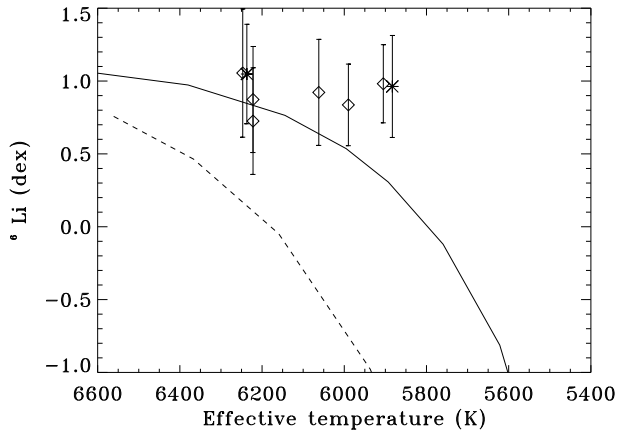


Fig. 3.— ${}^6\text{Li}$ pre MS depletion in $[\text{Fe}/\text{H}]=-2$ dex (solid line) and $[\text{Fe}/\text{H}]=-1$ dex (dashed line). Each curve has been shifted upwards by 0.2 dex in order to account for microscopic diffusion effects. Diamonds: data in the $[\text{Fe}/\text{H}]=-1$ to -2 dex range from Asplund et al. (2005a) and M. Asplund private communication; Stars: data from Nissen et al. (1999) $[\text{Fe}/\text{H}] \approx -0.6$ dex.

tion : Ryan et al. (1996) report a ~ 0.04 dex ${}^7\text{Li}$ variation every hundred Kelvin. Second the scatter on the plateau is extremely small for field stars. Spite et al. (1996) find $\sigma_{\tau_{\text{Li}}} \sim 0.06 - 0.08$ dex, Bonifacio & Molaro (1997) find $\sigma_{\tau_{\text{Li}}} \sim 0.07$ dex, while Melendez & Ramirez (2004) find $\sigma_{\tau_{\text{Li}}} \sim 0.06$ dex and Ryan et al. (1999) find $\sigma_{\tau_{\text{Li}}} \leq 0.02$ dex. Given the observational errors the scatter is in any case considered consistent with zero by the authors and clearly lies well below 0.1 dex⁵.

We compute the MS evolution of ${}^7\text{Li}$ for $[\text{Fe}/\text{H}]=-2$ dex models (composition described in detail in tables 1 & 2). The rotation law is that of case A : $K = K_{\odot}$, and $\tau_{\text{d}} = 3$ Myr (see §3). We stress however that a different early rotation history has no impact on the MS tachocline mixing and therefore on the surface lithium evolution. The reason stems from the swiftly converging rotational velocities after a few megayears combined with the few megayear the tachocline mixing requires for its onset. In our approach the surface abundances are not sensitive to the ZAMS angular momentum content. In spite of a wide

⁵The scatter observed in globular clusters such as M92 is higher (Boesgaard et al. 1998) and probably induced by the interactions resulting from the denser stellar environment.

range of possible early rotation histories the late MS ${}^7\text{Li}$ contents will show no resulting scatter. Even if we exceptionally consider the effect of the tachocline mixing to start as early as 50 Myr, differences resulting from early rotation differences (i.e. the different initial angular momentum amounts) would not be significant. In this situation the difference in ${}^7\text{Li}$ fraction we compute between the case of a slow and a fast ZAMS rotation (case A and B respectively on figure 1) is 0.04 dex at $T_{\text{eff}} = 5270$ K and gets smaller above this temperature. Figures 4 and 5 present our results along with observations. The observational data have been taken from Ryan et al. (1996), Ryan, Norris & Beers (1999), Ryan et al. (2001), Melendez & Ramirez (2004) and Charbonnel & Primas (2005). In order to diminish the possible ${}^7\text{Li}$ trends with $[\text{Fe}/\text{H}]$ we selected stars with metallicity between -2.5 and -1.5 for the plateau objects ($T_{\text{eff}} \geq 5500\text{K}$). Below $T_{\text{eff}} = 5500\text{K}$ we use the data from Ryan & Deliyannis (1998) and Thorburn (1994). To keep a reasonable number of stars in this region we considered a less restrictive criterium on the metallicity and extended the sample to objects having $-3 < [\text{Fe}/\text{H}] < -1$. We carefully excluded the subgiants from the sample using the recent work of Charbonnel and Primas (2005). This work takes advantage of the HIPPARCOS parallaxes in determining the stellar evolutionary status. All the objects considered in figures 4 and 5 are dwarfs or turn-off stars and comply with our prescriptions on metallicity. However the four objects having upper limits in lithium detection and T_{eff} above 5900 K have $-1.66 \text{ dex} < [\text{Fe}/\text{H}] < -0.88 \text{ dex}$. Only one of them is a confirmed dwarf (see table 5). Nevertheless because of their high effective temperature these stars, if subdwarfs, have not experienced any significant additive extension of their outer convection zone since the turn-off. Thus their surface lithium fraction is not expected to have changed since the main sequence. The computations have been made with both tachocline and microscopic diffusion or only microscopic diffusion. In any case a ${}^7\text{Li}$ plateau is predicted above 5500 K. This plateau lies between 0.2 and 0.4 dex below the initial abundances. In the microscopic diffusion models the abundances moreover decrease by 0.2 dex between 5700 K and the hotter end of the plateau near 6400 K. On the plateau the main

effect of the tachocline mixing is to correct this effective temperature dependence : only a small decrease of less than 0.1 dex in ${}^7\text{Li}$ remains towards the hot edge of the plateau. These computations are in agreement with the predictions of Richard et al. (2005): on the one hand the microscopic diffusion plays the major role in determining the level of the plateau, on the other hand the shape of the plateau requires that a non standard mixing process occurs in the radiation zone. For the sake of clarity the tachocline mixing models built with the highest rotation velocity of the radiation zone (case D) do not appear on figure 4. Above 6000 K these models do not show differences in ${}^7\text{Li}$ exceeding 0.1 dex with the predictions of case A rotation models. In the framework of the tachocline mixing the most rapid rotation rates inferred from HB fast rotators are thus unable to explain the lithium poor stars near the turn off. We shall return to this question in the next chapter. Below 5700 K the tachocline mixing models provide an explanation of the observed ${}^7\text{Li}$ pattern. On the contrary the pure microscopic diffusion models do not predict any ${}^7\text{Li}$ depletion around 5500-5400 K. The tachocline mixing therefore improves the situation with respect to pure microscopic diffusion models. However there are still two remaining issues. First the observed plateau still lies 0.2 dex below the predictions. Second the abundances below 5500 K appear largely scattered at a given effective temperature.

A possible explanation of the discrepancy between the observed and predicted plateau may stem from a slight underestimation of ${}^7\text{Li}$. It has been suggested recently by Melendez & Ramirez (2004) that such an underestimate could be related to an incorrect evaluation of the T_{eff} scale. The ${}^7\text{Li}$ abundance inferred by these authors is 2.37 dex which is in perfect agreement with our predictions as shown on figure 5. These observational results however still have to be confirmed. What is the origin of the scatter in lithium abundances at a given T_{eff} ? on the cooler side of the plateau? As we have seen in §4, metallicity effects and pre MS structural evolution are unable to explain this scatter. If one then investigates the effects of a MS rotational mixing process it is tempting to relate the lithium scatter to different rotation histories. However, several clues coming from population I observations lead us to think

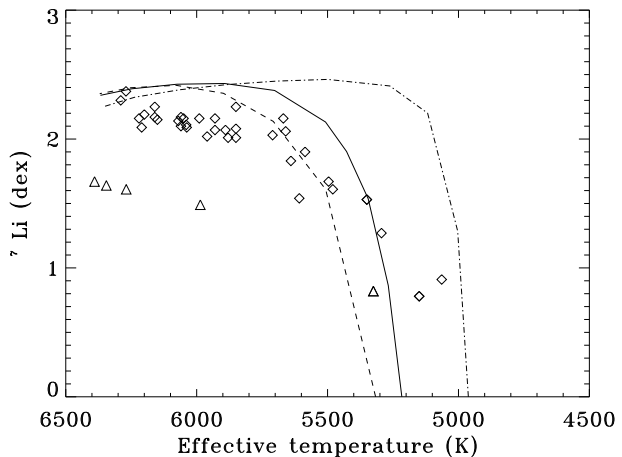


Fig. 4.— $T_{\text{eff}}-{}^7\text{Li}$ MS relation in tachocline models of buoyancy frequency $10 \mu\text{Hz}$ (solid line) and $2 \mu\text{Hz}$ (dashed line). The ${}^7\text{Li}$ depletion pattern is also provided for pure microscopic diffusion models (dot-dashed line). The age of the models is 13 Gyr, they all have the standard composition ($[\text{Fe}/\text{H}]=-2$ dex). The data are the same as in figure 2.

that this is an incorrect interpretation. For instance, the Hyades solar-like stars are slow rotators with $v_{\text{ini}} < 10 \text{km.s}^{-1}$. They presumably have experienced very different rotation histories as is suggested by the observations of younger clusters. However they show almost no scatter of their lithium abundances at a given temperature between 5000 and 6000 K (see for instance fig 6 of Thorburn et al. 1993). Therefore in the case of the Hyades it appears artificial to relate differences of initial angular momentum and differences of lithium abundances. One could imagine that the Hyades solar analogs have kept radiative cores rotating with various speeds from their early evolution and that the subsequent loss of angular momentum will induce different amounts of mixing and surface lithium destruction. However the presence of fast rotating cores and slow rotating envelopes after the Hyades age is not supported by helioseismic or early rotation history constraints. As we mentioned in chapter 3, solid body rotation is probably achieved at the Hyades age. If this is correct, the tachocline mixing (or any other rotation induced mixing) combined with the microscopic diffusion will produce similar effects on lithium during the subsequent evolution. We sug-

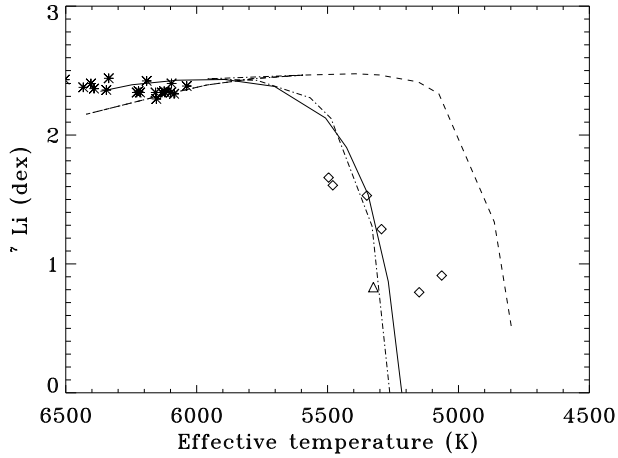


Fig. 5.— $T_{\text{eff}} - {}^7\text{Li}$ MS relation in tachocline models of buoyancy frequency $10 \mu\text{Hz}$. The ${}^7\text{Li}$ depletion pattern is provided for $[\text{Fe}/\text{H}]=-2$ dex (solid line), $[\text{Fe}/\text{H}]=-3$ dex (dot-dashed line), $[\text{Fe}/\text{H}]=-2$ with the solar repartition among metals (dashed line). The age is 13 Gyr. Note the significant impact of the metal repartition on the lithium depletion. The data have been taken considering the stars having $-2.5 < [\text{Fe}/\text{H}] < -1.5$ of the sample of Melendez & Ramirez (2004) observations (star symbols) plus Ryan & Deliyannis (1998) and Thorburn (1994) for objects below 5500 K in T_{eff} (diamonds).

gest the lithium scatter originates in differences of the metal content instead. The relevant quantity is not $[\text{Fe}/\text{H}]$ however: as shown on figure 5 tachocline models with $[\text{Fe}/\text{H}]=-2$ dex or $[\text{Fe}/\text{H}]=-3$ dex exhibit the same depletion pattern. The abundance repartition among metals has a much stronger influence on lithium. *The models keeping $[\text{Fe}/\text{H}]=-2$ dex but with solar repartition among metals are less lithium depleted for any given effective temperature than the models assuming a population II metal distribution.* Changing the oxygen to iron ratio by 0.3 dex affects the ${}^7\text{Li}$ content more at a given effective temperature than changing the global metallicity by 1 dex. Figure 6 displays the BCZ temperatures as a function of the effective temperatures for the three compositions displayed on figure 5. The relation is more affected by a change in the metal ratios than by a change in the total metal fraction. The solar metal repartition models exhibit considerably lower BCZ temperatures at any given effective temperature. The rea-

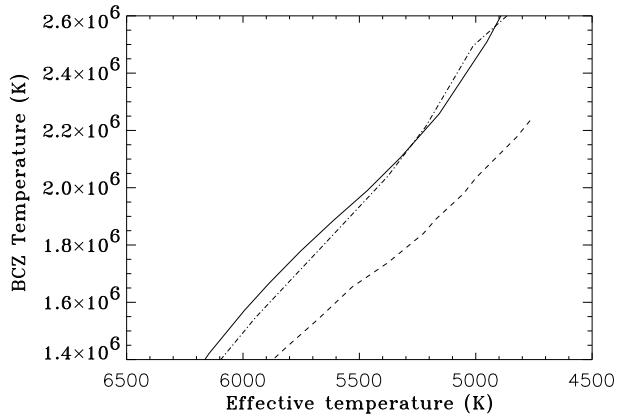


Fig. 6.— $T_{\text{eff}} - T_{\text{BCZ}}$ relation in the models of $[\text{Fe}/\text{H}]=-2$ dex, $[\text{Fe}/\text{H}]=-3$ dex and $[\text{Fe}/\text{H}]=-2$ with the solar repartition among metals. Linestyle conventions are the same as in figure 5. Note the huge impact of metal repartition on the relation.

son for this behavior is twofold. The iron tunes the opacity near the top part of the convection zone whereas the oxygen tunes the opacity near the base of the convection zone. Figure 7 illustrates these opposite behaviors for a model where ${}^7\text{Li}$ depletion becomes significant ($T_{\text{eff}} = 5270\text{K}$). An increase of the iron fraction tends to increase the thermal gradient $\nabla = \frac{d \ln T}{d \ln P}$ in the superadiabatic region and thus tends to increase the entropy of the deep convection zone. In turn this decreases the depth of the convection zone. If the iron content is fixed so is the entropy of the convection zone and the position of the BCZ then becomes very sensitive to the opacity in this region. The oxygen being the main opacity contributor near the BCZ, a diminution of the oxygen content at fixed $[\text{Fe}/\text{H}]$ will induce a drop of BCZ temperature as illustrated on figure 6. The oxygen to iron fraction drops by a factor 2 from the population II to the population I metals repartition, this in turn translates into a smaller ${}^7\text{Li}$ depletion (figure 5).

Because of the combined opacity roles of oxygen and iron we predict a correlation between ${}^7\text{Li}$ abundance and $[\text{Fe}/\text{O}]$. We expect this correlation only below 5500 K and moreover for objects having $[\text{Fe}/\text{H}]$ above ~ -2 dex. If the T_{eff} condition is not fulfilled the BCZ is not close enough to the regions where ${}^7\text{Li}$ nuclear burning can occur. Alternatively if the $[\text{Fe}/\text{H}]$ condition is not fulfilled

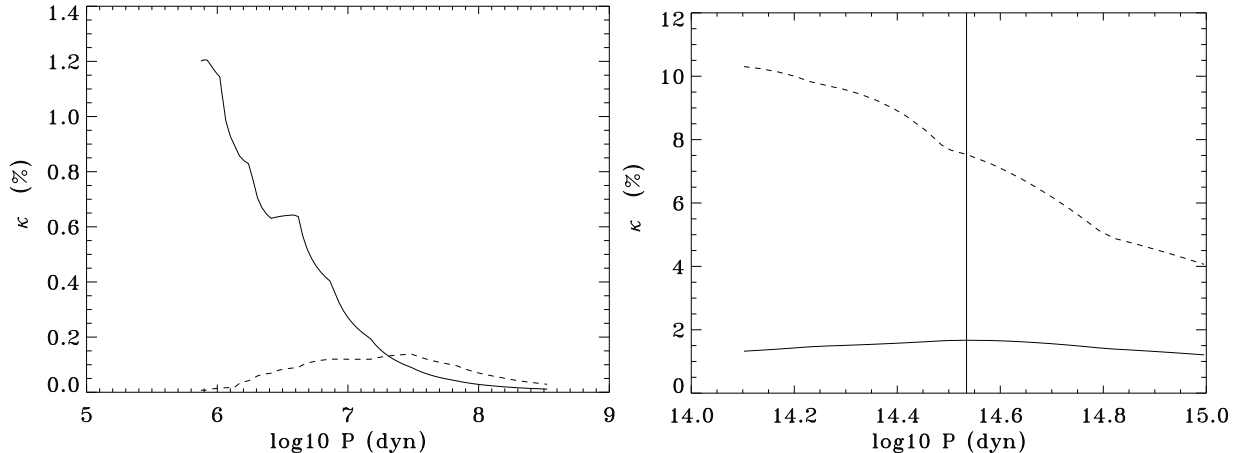


Fig. 7.— Left panel: opacity contributions in % for iron (solid line) and CNO (dashed line) as function of the pressure in the upper convection zone. The computations are for the $0.62M_{\odot}$ ($T_{\text{eff}} = 5260\text{K}$) at 13 Gyr with $[\text{Fe}/\text{H}]=-2$ dex and halo repartition among metals. The superadiabatic region extends down to $\log P=7$. Right panel : opacity contributions for iron and oxygen as a function of the pressure in the lower convection zone. The linestyles are similar to the upper panel. The vertical line shows the BCZ.

the metals do not have enough impact on the stellar structure to induce differences in the history of ${}^7\text{Li}$. In this respect the anti-correlation between $[\text{Fe}/\text{O}]$ and ${}^7\text{Li}$ observed in NGC6752 by Pasquini et al. (2005) does not contradict our expectations because it concerns turn-off stars ($T_{\text{eff}} > 5900\text{K}$). Following these authors we think that the chemical properties of these objects are related to the material that formed them. The case of a recently studied star HE1327-2326 (Frebel et al. 2005) also drew our attention. With an effective temperature of $6180 \pm 80\text{K}$, HE1327-2326 should lie on the lithium plateau. It is currently the lowest metallicity star known: $[\text{Fe}/\text{H}]=-5.4$ dex. However it is found to be anomalously lithium poor, the upper limit being $[{}^7\text{Li}]=1.6$ dex. The metal distribution in this object differs significantly from other population II dwarfs : e.g. $[\text{O}/\text{Fe}]$ could be as high as 3.7 dex for this star and $[\text{C}/\text{Fe}]=3.9$ dex. Considering the composition observed in this star⁶ we have tested the tachocline mixing model for $T_{\text{eff}} = 6200$ K. Despite a large oxygen fraction, we found no significant depletion of ${}^7\text{Li}$ at 13 Gyr. Because of the very small metallicity the effects of the metals are quite moderate on HE1327-2326

⁶The helium mass fraction was assumed 0.2479 while the oxygen and all the metals not mentioned in Frebel et al. (2005) were set to $[\text{X}/\text{Fe}]=3.7$ dex.

even though $[\text{O}/\text{Fe}]$ is huge. This illustrates the $[\text{Fe}/\text{H}]$ condition we mentioned just before. In this respect it is interesting to note that the heavy elements mass fraction and $[\text{O}/\text{H}]$ ratio we compute for HE1327-2326 are $Z = 3.1 \cdot 10^{-4}$ and -1.8 respectively which is comparable to our standard composition case where $Z = 3.0 \cdot 10^{-4}$ and $[\text{O}/\text{H}]=-1.7$ dex (see table 1).

5.2. Below the ${}^7\text{Li}$ plateau

About 7% of the halo turn-off stars are lithium poor with abundances below 1.7 dex. Some of these objects show peculiar chemical abundance patterns while some others cannot be distinguished from the other 'normal' lithium abundance stars. However the majority of these stars clearly rotates faster than their Li-normal counterparts (Ryan & Elliott 2005). At first sight this point should once again suggest a connection between lithium and rotation effects. However we do not think that these stars are lithium poor because they reached the ZAMS with more angular momentum. The distribution of rotational periods in ZAMS open-clusters such as IC2602 and IC2391 do not show a small fraction of stars, say between 5 and 10 %, having periods clearly shorter than the bulk of other comparable objects. It rather seems that rotation periods are uniformly

distributed on the 0.2-10 days range (Barnes et al. 1999). If the ZAMS rotation distribution was responsible for lithium poor halo dwarfs at turn-off, one would expect more stars below the plateau and a continuous distribution of them as function of the lithium fraction. This is not the case: hot lithium poor stars are rare and there is an observational gap of objects between $[^7\text{Li}] \approx 2.1$ dex and the upper limit of 1.7 dex. Furthermore the Li-poor objects generally belong to binary systems. Indeed three out of four Li-poor stars of the Ryan et al. (2002) sample are confirmed binaries, the secondary component being presumably a compact object. This leads the authors to assume the higher rotation rates were achieved through angular momentum accretion accompanying a mass transfert from the former primary component. Several processes could account for the low lithium fraction : the variation of rotation rate and angular momentum of the accreting object may have induced enough internal mixing. Alternatively the accreted matter may have been initially lithium poor and induced a subsequent dilution.

Our purpose here is to briefly check these two possibilities in the case where one considers the tachocline diffusion as the rotation induced mixing process. Table 5 shows the Ryan et al. (2002) data for their Li-poor stars while the table 6 provides the general characteristics of our models computed for $[\text{Fe}/\text{H}]=-1$ dex, more or less the metallicity of the observed objects. Out of the four objects of table 5, CD-3119466 might be peculiar: it is neither a confirmed fast rotator nor a spectroscopic binary and is further away from turn-off than the other stars. On this basis we exclude it from the subsequent discussion. Table 6 shows that the masses of the observed Li-poor stars probably lie between 0.8 and $0.86M_{\odot}$. Masses above $0.9 M_{\odot}$ are excluded unless the stars are evolving towards the subgiant stage and already have at least lost ≈ 160 K since the turn-off. Moreover such high masses would mean that the Li-poor objects have half the age of the typical halo stars. Masses below $0.8 M_{\odot}$ also seem excluded because such objects should not reach the high observed effective temperatures.

Now that the plausible mass range for lithium poor objects is established let us consider the effect of the tachocline mixing. Ryan et al. (2002) es-

timate a typical mass increase of $10^{-2}M_{\odot}$. Thus the masses of the lithium poor progenitors were probably well above $0.75 M_{\odot}$ ($T_{\text{eff}} = 5700\text{K}$ on the ZAMS). Prior to the mass transfert these stars were hot enough to be on the plateau and to have a 'normal' ^7Li fraction. The depletion impact of the tachocline mixing on a $0.8 M_{\odot}$ star is negligible even for a high angular rotation velocity. We built a $0.8 M_{\odot}$ model with constant rotation rate $1.27 \cdot 10^{-5} \text{rad.s}^{-1}$ on the MS. This rate is chosen such that at 13 Gyr the surface equatorial velocity is 10 km.s^{-1} which is the order of magnitude of the velocity suggested by the vsini measurements (table 5). However this model is extreme in terms of rotation and tachocline mixing because it keeps a high angular velocity all along its evolution. We find that the final ^7Li of this model is 2.32 dex. Despite the high rotation rate no depletion occurs because the region of nuclear lithium burning lies too deep below the base of the convection zone.

Let us now consider the effect of lithium dilution. As can be seen in table 6 the masses of the outer convection zones of the considered objects are quite small. If the total mass of the ^7Li object is close to $0.8 M_{\odot}$ then a $3 \cdot 10^{-2}M_{\odot}$ mass transfert of lithium free material would be necessary to dilute the ^7Li below the observed upper limits and down to $[^7\text{Li}]=1.61$ dex. Alternatively if the mass is close to $0.86 M_{\odot}$ then a $10^{-2}M_{\odot}$ accreted mass would be enough to decrease lithium to $[^7\text{Li}]=1.55$ dex. Therefore the dilution mechanism of ^7Li can explain the low lithium surface abundances observed in some turn-off halo dwarfs. The need for an additive mixing process is required only if the accreted mass is below $10^{-3}M_{\odot}$. Then the decrease in surface lithium fraction would be less than 0.2 dex even in the lighter case we estimate for the convection zone. We note furthermore that in this case the process responsible for the mixing could not possibly be the tachocline mixing. Abundance measurements of other elements than ^7Li would certainly clarify the issue of the origin of near turn-off ^7Li deficient stars. For instance the detection of higher nitrogen and lower carbon fractions than in the 'normal' halo dwarfs would support the accretion scenario from a red giant star. The conversion of carbon into nitrogen is ascribed to deep mixing and is clearly observed from moderately (Smith, Briley & Harbeck 2005) to extremely (Spite et al. 2005) metal

Table 5: Turn off lithium poor objects. Data from Ryan et al. (2001) and Ryan et al. (2002). These stars appear in figure 2 and 4. Charbonnel & Primas (2005) showed that Wolf 550 is a dwarf and G202-65 is a subgiant. The two other stars are not mentioned by this work.

Object	vsini (km.s ⁻¹)	T _{eff} (K)	[Fe/H] (dex)	⁷ Li (dex)
CD-31 19466	< 2.2	5986	-1.66	< 1.49
Wolf 550	5.5 ± 0.6	6269	-1.56	< 1.61
BD +51 1817	7.6 ± 0.3	6345	-0.88	< 1.64
G202-65	8.3 ± 0.4	6390	-1.32	< 1.67

Table 6: [Fe/H]=-1dex models characteristics at their maximum MS effective temperature.

Mass (M _⊙)	T _{eff} (K)	age (Gyr)	Mass of the convection zone (M _⊙)
0.80	6233	12.15	6.5 10 ⁻³
0.83	6326	10.25	3.6 10 ⁻³
0.86	6426	8.73	1.9 10 ⁻³
0.90	6548	7.10	7 10 ⁻⁴

poor giants. The presence of ⁶Li in these otherwise ⁷Li poor objects would also favour the accretion scenario because it is difficult to imagine how this more fragile isotope could survive if ⁷Li experienced enhanced proton capture.

5.3. Predictions on ⁶Li

The region of nuclear destruction of ⁶Li is close to the lower limit of the outer convection zone in halo dwarf stars. In this respect ⁶Li provides tighter constraints than ⁷Li on these objects. Figure 8 is the equivalent for ⁶Li to figure 4 for ⁷Li. The data are those mentioned in §4. We stress that not all the stars are confirmed as dwarfs by the recent analysis of Charbonnel & Primas (2005). However the subgiants of the sample are all hot enough that no significant dilution or nuclear destruction of ⁶Li is expected from deeper convective zones. Two tachocline diffusion models are displayed for [Fe/H]=-2 and halo star metal repartition and for [Fe/H]=-2 and solar metal repartition. Above 6000 K the agreement with the data is good for the two sets of models. Because the turbulence induced by tachocline

mixing is shallow, both models brake diffusion of heavy elements around the turn-off without inducing significant ⁶Li destruction here. This is an improvement with respect to the computations of Richard et al. (2005). Nonetheless below 6000 K the tachocline models for the composition expected for halo stars predicts too strong a depletion. The presence of ⁶Li in stars as cool as 5900 K appears problematic. However no hasty conclusion should be drawn because of the complexity of the situation. First, non detection stars are not represented on the plot. We recall that for the Asplund et al. (2005a) sample only 9 out of 24 stars yielded to an unambiguous ⁶Li detection. Second because of the still rare ⁶Li detections, the data of stars having -2 < [Fe/H] < -1 dex are compared to the models. For the sake of simplicity we consider a unique ⁶Li initial fraction (≈ 1.1 dex after correction for diffusion effects). However cosmic ray activity predicts a significant increase of ⁶Li over the actual metallicity range (Rollinde et al. 2005). Finally we expect that the metal repartition effects will change the effective temperature/BCZ temperature relation as aforemen-

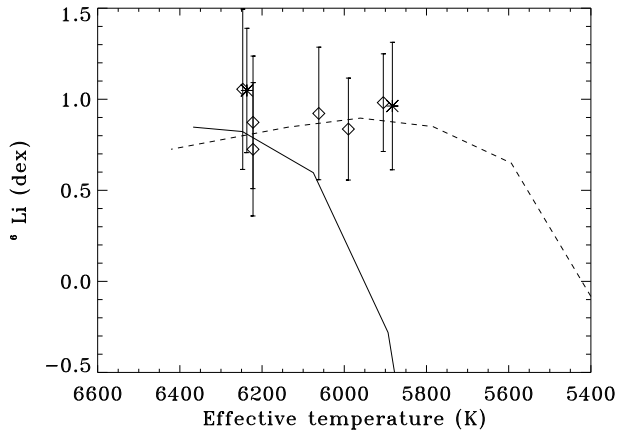


Fig. 8.— $T_{\text{eff}} - {}^6\text{Li}$ relation for tachocline diffusion models of buoyancy frequency 10μ Hz. Solid line: $[\text{Fe}/\text{H}]=-2$ dex and halo repartition among metals. Dashed line $[\text{Fe}/\text{H}]=-2$ dex and solar repartition among metals. The data and error bars are from Asplund et al. (2005a) (diamonds) and Nissen et al. (1999) (star symbols).

tioned. In the same manner as in the preceding chapter we considered the tachocline mixing impact when $[\text{Fe}/\text{H}]=-2$ dex and the metal repartition is solar. As can be seen on figure 8 the agreement to the data is then quite improved. This suggest there should be a $[\text{Fe}/\text{O}]$ to ${}^6\text{Li}$ correlation for halo dwarfs around the turn-off.

6. Summary

We examined in detail the evolution of both lithium isotopes in halo stars of effective temperatures in the 4700 to 6500 K range. Their depletion history has been followed during the pre main sequence and the main sequence up to the age of 13 Gyr and compared with observations. The ${}^9\text{Be}$ history was also followed but no significant evolution of this species is predicted because of its higher temperature for proton capture compared to lithium. Our models include the most recent physics (§2) in terms of equation of state and opacities (OPAL tables), nuclear reaction rates (NACRE compilation) and atmospheric boundary conditions (NextGen atmosphere models). Special attention was given to the metal fractions impact through opacity effects: models with $[\text{Fe}/\text{H}]=-3, -2, -1$ and -0.7 dex have been considered. In all cases the helium mass fraction and ${}^7\text{Li}$

number fraction were assumed to be primordial: $Y=0.2479$ and $[{}^7\text{Li}]=2.62$ dex respectively (Coc et al. 2004). The initial ${}^6\text{Li}$ number fraction was assumed to be 1.13 dex. The microscopic diffusion has always been taken into account. Moreover we have studied the effects of the tachocline turbulent diffusion, a rotationally induced mixing that was previously demonstrated to explain lithium and beryllium history in the Sun and other population I stars. The two free parameters of the tachocline diffusion process are calibrated on the Sun (§3). The rotation history of a $0.7 M_{\odot}$ model is used to account for the tachocline mixing. This rotation history was computed in detail, taking into account the structural changes and surface angular momentum losses (§3).

During the pre main sequence all the models evolve from a fully convective stage to a radiative core / convective envelope structure. Meanwhile the temperature at the boundary between these two regions reaches a maximum. The peak temperature increases as the mass of the star decreases which results in an enhanced lithium depletion on the ZAMS for cooler objects. As is well known, the observed ${}^7\text{Li}$ abundance pattern shows a plateau in ${}^7\text{Li}$ vs T_{eff} from the turn-off down to $T_{\text{eff}} \approx 5500$ K while below this value the depletion gradually increases with decreasing effective temperature. We showed that this pattern cannot be explained by pre main sequence depletion regardless of metallicity below $[\text{Fe}/\text{H}]=-1$ dex (§4). The predictions of depletion are at least 0.7 dex above the observations in the effective temperature range between 5500 K and 5000 K. Thus an additive non standard mixing process in the radiation zone is necessary to explain the present day observations. It is noteworthy that, contrary to the population I case, the ZAMS predicted $T_{\text{eff}} - {}^7\text{Li}$ relation does not depend on the metal content. ${}^6\text{Li}$ abundance provide additional informations about the pre main sequence evolution. The expected depletion of this isotope depends on the metallicity and clearly exceeds what is observed in some halo dwarfs. This issue is similar to what we found in earlier work for population I star with respect to ${}^7\text{Li}$ pre main sequence depletion (PTC02). For surface temperatures cooler than 6000 K some stars are observed on their late main sequence with a ${}^6\text{Li}$ content at least 1.5 dex above pre main sequence predictions. This indicates that the initial conditions or

the early structural changes of population II stars are not understood.

The pre main sequence results show that a non-standard main sequence mixing near the base of the convection zone is necessary to explain the ${}^7\text{Li}$ fraction below $T_{\text{eff}} = 5500$ K. The $T_{\text{eff}} - {}^7\text{Li}$ relation calculated with microscopic diffusion models at 13 Gyr also suggest that a turbulent process prevents too efficient microscopic diffusion near the turn-off. The tachocline mixing provides good results for the ${}^7\text{Li}$ abundance pattern on the cool side of the plateau. Moreover as the phenomenon creates turbulence below the convection zone it also prevents increased depletion where the microscopic diffusion timescale becomes shorter. Consequently the Spite plateau is well reproduced (§5). Its average level lies between 2.4 and 2.3 dex. This is slightly above the bulk of the observations, but in perfect agreement with the recent results of Melendez & Ramirez (2004). We showed that the early main sequence rotation history has no impact on ${}^7\text{Li}$ provided that nearly solid body rotation is efficiently enforced in low mass stars. There are indeed several observational clues that the solid body rotation is rapidly achieved in low mass stars. Furthermore using constraints from horizontal branch stars rotation we showed that even if halo dwarfs keep fast rotating cores this should not induce increased lithium depletion around turn-off. The tachocline mixing requires a few gigayears to become effective whereas solid body rotating stars achieve similar rotation rates after ≈ 0.2 Gyr. Consequently the small scatter on the ${}^7\text{Li}$ plateau is not contradictory with scattered rotational rates on the ZAMS even if one considers that the turbulence below the convection zone is connected to rotation. In the framework of the tachocline mixing the initial angular momentum and the surface abundances are not correlated. The tachocline mixing is robust with respect to the new observations. It predicts ${}^6\text{Li}$ abundances in agreement with the observations above 6000 K. The rare objects exhibiting a ${}^7\text{Li}$ abundance clearly below the plateau and an effective temperature above 6000 K cannot be explained in the framework of the tachocline process despite their abnormally high rotation rates. We show however that because of their light convection zones, accretion of lithium free matter below a few percent of solar mass could explain the actual

observations. The detection of ${}^6\text{Li}$ or enhanced nitrogen content in these objects would be strong support in favor of such an accretion scenario from an evolved star. We suggest that the scatter in ${}^7\text{Li}$ for stars cooler than the red edge of the Spite plateau is related to differences in the metal repartition in the stars instead of different rotation histories. The variation of the metals ratio from population II repartition to population I repartition *at fixed T_{eff}* significantly diminishes lithium depletion. We predict a correlation between $[\text{Fe}/\text{O}]$ and lithium abundance in both isotopes at any given effective temperature below 5500 K for ${}^7\text{Li}$ and 6000 K for ${}^6\text{Li}$. These correlations should be observed in dwarfs stars where the metal repartition goes from halo repartition to disk repartition (i.e. around $[\text{Fe}/\text{H}] = -1.5$ dex). To our knowledge such correlations have not yet been investigated.

REFERENCES

- Akerman, C.J., Carigi, L., Nissen, P.E., Pettini, M., & Asplund, M., 2004 A&A, 414, 931
- Alexander, D. R., Ferguson, J. W., 1994, ApJ, 437, 879
- Angulo, C., et al., Nucl. Phys. A656 (1999)3-187
- Asplund, M., Nissen, P. E., Lambert, D. L., Primas, F., Smith, V. V., 2005a, Proceedings of IAU symposium 228, Ed. V. Hill, P. François, F. Primas.
- Asplund, M., Nissen, P. E., Lambert, D. L., Primas, F., Smith, V. V., 2005b, submitted to ApJ
- Bahcall, J. N., Pinsonneault, M. H., Wasserburg, G. J., 1995, RvMP, 67, 781
- Barnes, S. A., Sofia, S., Prosser, C. F., Stauffer, J. R., 1999, ApJ, 516, 263
- Behr, B. B., 2003, ApJSS, 149,67
- Böhm-Vitense, E., 1958, Zs. f. Ap., 46, 108
- Bonifacio, P., Molaro, P., 1997, MNRAS, 285, 847
- Boesgaard A. M., Deliyannis, C. P., Stephens, A., King, J. R., 1998, ApJ 493, 206
- Bouvier, J., Forestini, M., Allain, S., (BFA97) 1997, A&A, 326, 1023

- Brun, A. S., Turck-Chièze, S., Zahn, J. P. 1999, *ApJ*, 525, 1032
- Brun, A. S.; Antia, H. M., Chitre, S. M., Zahn, J.-P., 2002, *ApJ*, 391, 725
- Burles, S., 2002, *P&SS*, 50, 1245
- Cayrel, R., Spite, M., Spite, F., Vangioni-Flam, E., Cass, M., Audouze, J., 1999, *A&A*, 343, 923
- Cayrel, R., Depagne, E., Spite, M., Hill, V., Spite, F., François, P., Plez, B., Beers, T., Primas, F., Andersen, J., and 4 coauthors, 2004, *A&A*, 416, 1117
- Charbonnel, C., Primas, F., 2005, *A&A*, accepted
- Cyburt, R. H., Fields, B. D., Olive, K. A., 2004, *Phys. Rev. D*, 69, 123519
- Cyburt, R. H., Fields, B. D., Olive, K. A., 2003, *Phys. Lett. B*, 567, 227
- Donahue, R. A., Saar, S. H., Baliunas, S. L., 1996, *ApJ*, 466, 384
- Frebel, A., Aoki, W., Christlieb, N., Ando, H., Asplund, M., Barklem, P. S., Beers, T. C., Eriksson, K., Fechner, C., Fujimoto, M. Y., and 9 coauthors, 2005, *Nature*, 434, 871
- Gratton, R. G., 1989, *A&A*, 208, 171
- Hobbs, L. M., Duncan, D. K., 1987, *ApJ*, 317, 796
- Iglesias, C. A., & Rogers, F., J., 1996, *ApJ*, 464, 943
- Magain, P., 1989, *A&A*, 209, 211
- Melendez, J., Ramirez, Y, 2004, *ApJ*, 615, 33
- Michaud, G., Proffitt, C. R., 1993, *Inside the stars*, IAU colloquium, 137, ASP Conference series, eds. A. Baglin, & W. W. Weiss vol 40, 426
- Montalbán, J. & Schatzman, E., 2000, *A&A* 354, 943
- Morel, P., 1997, *A&AS*, 124, 597
- Nissen, P. E., Lambert, D. L., Primas, F., Smith, V. V., 1999, *A&A*, 348, 211
- Pasquini, L., Bonifacio, P., Molaro, P., Francois, P., Spite, F., Gratton, R. G., Carretta, E., Wolff, B., 2005, *A&A*, 441, 549
- Piau, L., & Turck-Chièze, S., (PTC02) 2002, *ApJ*, 566, 419
- Piau, L., Randich, S., & Palla, F., 2003, *A&A*, 408, 1037
- Piau, L., Ballot, J., & , Turck-Chièze, S., 2005, *A&A*, 430, 571
- Proffitt, C. R., Michaud, G., 1991, *ApJ*, 371, 584
- Reeves, H., Fowler, W. A., Hoyle, F., 1970, *Nature*, 226, 727
- Rogers, F. J., Nayfonov, A., 2002, *ApJ*, 576, 1074
- Ryan, S. G., Beers, T. C., Deliyannis, C. P., Thorburn, J. A., 1996, *ApJ* 458, 543
- Ryan, S. G., Deliyannis, C. P., 1998, *ApJ*, 500, 398
- Ryan, S. G., Norris, J. E., Beers, T. C., 1999, *ApJ*, 523, 654
- Ryan, S. G.; Kajino, T., Beers, T. C., Suzuki, T. K., Romano, D., Matteucci, F. Rosolankova, K., 2001, *ApJ* 549, 55
- Ryan et al. 2002, *ApJ*, 571, 501
- Smith, V. V., Lambert, D. L., Nissen, P. E., 1998, *ApJ*, 506, 405
- Smith, G. H., Briley, M. M., Harbeck, D., 2005, *AJ*, 129, 1589
- Spiegel, E. A., Zahn, J.P., 1992, *A&A*, 265, 106
- Spite, F., Spite, M., 1982, *A&A* 115, 457
- Spite, F., Spite, M., 1993, *A&A* 279, L9
- Spite, M., Francois, P., Nissen, P. E., Spite, F., 1996, *A&A* 307, 172
- Spite, M., Cayrel, R., Plez, B., Hill, V., Spite, F., Depagne, E., Franois, P., Bonifacio, P., Barbuy, B., Beers, T., and 4 coauthors, 2005, *A&A*, 430, 655
- Talon, S., Kumar, P., Zahn, J. P., 2002, *ApJ*, 574, 175

- Talon, S., Charbonnel, C., 2004, *A&A*, 418, 1051
- Thorburn, J. A., Hobbs, L. M., Deliyannis, C. P., Pinsonneault, M. H., 1993, *ApJ*, 415, 150
- Thorburn, J. A., 1994, *ApJ*, 421, 318
- Thompson, M. J., Christensen-Dalsgaard, J., Miesch, M. S., Toomre, J., 2003, *A&ARA*, 41, 599
- VandenBerg, D., 2000, *ApJS*, 129, 315
- Vangioni-Flam, E., Cassé, M., Cayrel, R., Audouze, J., Spite, M., Spite, F., 1999, *NewA*, 4, 245
- Ventura, P., Zeppieri, A., Mazzitelli, I., D'Antona, F., 1998, *A&A*, 331, 1011
- Zahn, J. P. , 2004, 'Hydrodynamic models of the tachocline', Cambridge University press.